

Joint estimation of Doppler frequency and directions in channel sounding using switched Tx and Rx arrays

Pedersen, Troels; Pedersen, Claus; Yin, Xuefeng; Fleury, Bernard Henri; Pedersen, R.; Bozinovska, B.; Hviid, A.; Jourdan, P.; Stucki, A.

Published in:
IEEE Global Telecommunications Conference, 2004. GLOBECOM '04.

DOI (link to publication from Publisher):
[10.1109/GLOCOM.2004.1378429](https://doi.org/10.1109/GLOCOM.2004.1378429)

Publication date:
2004

Document Version
Publisher's PDF, also known as Version of record

[Link to publication from Aalborg University](#)

Citation for published version (APA):
Pedersen, T., Pedersen, C., Yin, X., Fleury, B. H., Pedersen, R., Bozinovska, B., Hviid, A., Jourdan, P., & Stucki, A. (2004). Joint estimation of Doppler frequency and directions in channel sounding using switched Tx and Rx arrays. In *IEEE Global Telecommunications Conference, 2004. GLOBECOM '04.* (Vol. 4, pp. 2354 - 2360). IEEE Signal Processing Society. <https://doi.org/10.1109/GLOCOM.2004.1378429>

General rights

Copyright and moral rights for the publications made accessible in the public portal are retained by the authors and/or other copyright owners and it is a condition of accessing publications that users recognise and abide by the legal requirements associated with these rights.

- Users may download and print one copy of any publication from the public portal for the purpose of private study or research.
- You may not further distribute the material or use it for any profit-making activity or commercial gain
- You may freely distribute the URL identifying the publication in the public portal -

Take down policy

If you believe that this document breaches copyright please contact us at vbn@aub.aau.dk providing details, and we will remove access to the work immediately and investigate your claim.

Joint Estimation of Doppler Frequency and Directions in Channel Sounding Using Switched Tx and Rx Arrays

Troels Pedersen*, Claus Pedersen*, Xuefeng Yin*, Bernard H. Fleury*,
Rene R. Pedersen*, Biljana Bozinovska*, Asger Hviid*, Patrik Jourdan**, Andreas Stucki**¹

*Information and Signals Division, Department of Communication Technology, Aalborg University, DK-9220 Aalborg, Denmark

**Elektrobit AG, Rosswiesstrasse 29, CH-8608 Bubikon, Switzerland

Abstract—To save hardware equipment and reduce the effort to calibrate the system, channel sounding with Tx and Rx antenna arrays is commonly performed in a time division multiplexing (TDM) mode where the array elements are successively switched. We refer to this technique as TDM-MIMO (multiple-input multiple-output) channel sounding. A recent study [1] shows that the ISI-SAGE algorithm [2], [3] applied in combination with TDM-MIMO channel sounding makes it possible to extend the Doppler frequency (DF) estimation range (DFER) by a factor at least equal to the product of the element numbers of the Tx and Rx arrays compared to the traditionally used DFER. The extension is significant when arrays with large element numbers are employed.

In this paper we derive the signal model for TDM-MIMO channel sounding and report analytical investigations showing that the above DFER extension requires selection of switching modes (SMs) tailored to the array characteristics. The SM of a switched array is the temporal order in which the array elements are switched. In fact, the traditionally used SMs of uniform linear and planar arrays where the elements are switched according to their natural spatial ordering prove to be inappropriate as they lead to an ambiguity in the joint estimation of DF and directions. We also introduce the concept of normalized side-lobe level (NSL) associated to the SM of a switched array. We show that minimizing the NSL is a sensible criterion for the identification of SM leading to DF and direction estimates with nearly optimum performance in terms of root mean square estimation error. Finally experimental investigations illustrate the impact of the SM of a uniform planar array on the behaviour of the DF and direction of arrival estimates computed with the ISI-SAGE algorithm.

I. INTRODUCTION

Deploying multiple-element antennas at the transmitter (Tx) and the receiver (Rx) combined with space-time coding can substantially increase the capacity of mobile radio communication systems [4], [5] and [6]. A system or technique using multiple-element Tx and Rx antennas is called a multiple-input multiple-output (MIMO) system or technique. The design and optimization of MIMO communication systems require realistic models of the propagation channel that incorporate dispersion in direction or equivalently space selectivity jointly at both Tx and Rx sites. High-resolution parameter estimation has become an essential tool to extract the critical model parameters from measurement data. The improved-search-and-initialization space-alternating generalized expectation-maximization (ISI-SAGE) algorithm [2], [3] has recently been

proposed for joint estimation of the polarization matrix, relative delay, Doppler frequency (DF), direction, i.e. azimuth and co-elevation angles, of departure (DoD), and direction of arrival (DoA) of propagation paths between the Tx site and the Rx site. Experimental investigations in [2], [3] demonstrate the high potential of the algorithm for detailed propagation studies.

MIMO channel sounders commonly operate in a time-division multiplex (TDM) mode in order to save hardware equipment and reduce the effort to calibrate the system. The sounding signal is fed successively at the ports of the array elements at the Tx, and while any one of these elements transmits, the ports of the antenna elements at the Rx are sensed successively. We understand an element pair to be a pair containing an element of the Tx array in first position and an element of the Rx array in second position. A measurement cycle denotes the process where all element pairs are switched once. A cycle interval is the period separating the beginning of two consecutive measurement cycles. The separation between the beginning of two consecutive sensing periods within one measurement cycle is called the switching interval. The cycle rate and the switching rate are the inverses of the cycle interval and the switching interval respectively. Notice that the ratio of the switching rate to the cycle rate is at least equal to the product of the element numbers of the two arrays.

It was traditionally believed, that the maximum absolute DF that can be estimated using the TDM-MIMO sounding technique equals half the cycle rate. Therefore, by keeping the switching rate unchanged, large element numbers in the arrays result in a low cycle rate and consequently lead to a small DF estimation range (DFER). However, a recent study [1] has shown that the maximum absolute DF that can be estimated using the TDM-MIMO sounding technique actually equals half the switching rate. This enlarged DFER is independent of the element numbers of the arrays.

In this paper, we show that the extension of the DFER proposed in [1] may result in an ambiguity in the estimation of the DF and directions (DoD and DoA). The estimates of the path parameters are computed in the maximization (M-) step of the ISI-SAGE algorithm to be the solution that maximizes a given objective function. The ambiguity occurs when this objective function exhibits multiple maxima. This situation may happen when the DFER is enlarged from minus to plus half the switching rate depending on the switching mode (SM) and the characteristics (e.g. the layouts and the element radiation patterns) of the arrays. The SM of an array describes the temporal order in which the array elements are

¹A. Stucki was with Elektrobit AG at the time the work presented in this paper was performed. He is presently with Solcept AG, Lindenhofstrasse 28, CH-8624 Gruet-Gossau, Switzerland.

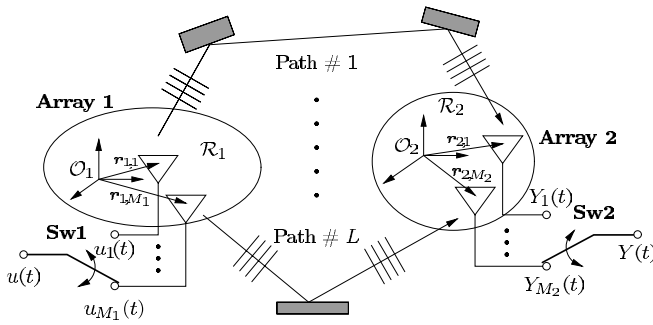


Fig. 1. Signal model for the TDM-MIMO sounding technique.

switched. This paper analyses the impact of the SMs of the arrays in TDM-MIMO sounding on the joint estimation of DF and directions using the ISI-SAGE algorithm by means of theoretical and experimental investigations combined with Monte-Carlo simulations.

The paper is organized as follows. The MIMO radio channel model is introduced in Section II. Section III presents the signal model for TDM-MIMO channel sounding. In Section IV the objective function used in the M-step of the ISI-SAGE algorithm is derived. Investigations of a case study considering TDM-SIMO (single-input multiple-output) channel sounding with a uniform linear array give insight into the ambiguity problem and the necessary and sufficient conditions for it to occur. In Section V the impact of the SM on the root mean square estimation errors (RMSEs) of the DF and DoA estimates is assessed via Monte Carlo simulations. In Section VI experimental investigations compare the performance of the DF and DoA estimators when applying the conventionally used SM and an optimized SM to a uniform planar array. Finally, concluding remarks are addressed in Section VII.

II. SIGNAL MODEL FOR MIMO SYSTEMS

Let us consider the propagation environment depicted in Fig. 1. A certain number, L , of waves propagate along different paths from the M_1 antenna elements forming Array 1 to the M_2 antenna elements forming Array 2. Along its path a wave interacts with a certain number of scatterers. We use the index $k \in \{1, 2\}$ for the arrays. Following [7], we assume that the far-field condition holds, and that the elements of Array k are confined in a region \mathcal{R}_k , in which the plane wave approximation is accurate. A coordinate system is specified at an arbitrary origin \mathcal{O}_k in \mathcal{R}_k . The individual locations of the elements of Array k are determined by the vectors $\mathbf{r}_{k,m} \in \mathbb{R}^3$, $m = 1, \dots, M_k$. Here, \mathbb{R} denotes the real line.

Let $\mathbf{u}(t) \doteq [u_1(t), \dots, u_{M_1}(t)]^T$ denote the (complex base-band representation of the) signal vector at the input of Array 1. Here, $[\cdot]^T$ is the transpose operator. The contribution of the ℓ th wave to the outputs of Array 2 can be written in vector notation as

$$\mathbf{s}(t; \boldsymbol{\theta}_\ell) = \alpha_\ell \exp\{j2\pi\nu_\ell t\} \mathbf{c}_2(\boldsymbol{\Omega}_{2,\ell}) \mathbf{c}_1(\boldsymbol{\Omega}_{1,\ell})^T \mathbf{u}(t - \tau_\ell). \quad (1)$$

In this expression, $\boldsymbol{\theta}_\ell \doteq [\boldsymbol{\Omega}_{1,\ell}, \boldsymbol{\Omega}_{2,\ell}, \tau_\ell, \nu_\ell, \alpha_\ell]$ is a vector whose entries are the parameters characterizing the ℓ th path: $\boldsymbol{\Omega}_{1,\ell}$, $\boldsymbol{\Omega}_{2,\ell}$, τ_ℓ , ν_ℓ , and α_ℓ denote, respectively its DoD, DoA, propagation delay, DF, and complex weight (or gain). We describe a direction as a unit vector $\boldsymbol{\Omega}$ with initial point anchored at the reference location, or equivalently as the terminal point of this vector, i.e. a point located on a unit

sphere centered at the reference point. Then, $\boldsymbol{\Omega}$ is uniquely determined by its spherical coordinates $(\phi, \theta) \in [-\pi, \pi) \times [0, \pi]$ according to $\boldsymbol{\Omega} = [\cos(\phi) \sin(\theta), \sin(\phi) \sin(\theta), \cos(\theta)]^T$. The angles ϕ and θ are referred to as respectively the azimuth and the co-elevation of $\boldsymbol{\Omega}$. The M_k -dimensional complex vector $\mathbf{c}_k(\boldsymbol{\Omega})$ represents the response of Array k to a wave impinging from direction $\boldsymbol{\Omega}$. Provided coupling effects between the array elements are negligible, $\mathbf{c}_k(\boldsymbol{\Omega}) = [f_{k,m}(\boldsymbol{\Omega}) \exp\{j\frac{2\pi}{\lambda_0}(\boldsymbol{\Omega}^T \mathbf{r}_{k,m})\}; m = 1, \dots, M_k]^T$. The function $f_{k,m}(\boldsymbol{\Omega})$ is the complex electric radiation patterns of the m th element in Array k , and λ_0 denotes the carrier wavelength.

The signal vector $\mathbf{Y}(t) \doteq [Y_1(t), \dots, Y_{M_2}(t)]^T$ representing the outputs of Array 2 is given by

$$\mathbf{Y}(t) = \sum_{\ell=1}^L \mathbf{s}(t; \boldsymbol{\theta}_\ell) + \sqrt{\frac{N_0}{2}} \mathbf{W}(t), \quad (2)$$

where $\mathbf{W}(t) \doteq [W_1(t), \dots, W_{M_2}(t)]^T$ is standard M_2 -dimensional complex temporally and spatially white Gaussian noise, and N_0 is a positive constant.

III. TDM CHANNEL SOUNDING TECHNIQUE

Sounding of the propagation channel is performed in a TDM mode according to the time structure depicted in Fig. 2. As depicted in Fig. 1, the sounding signal is fed via Switch 1 (Sw1) during a sounding period T_t successively to the ports of the elements of Array 1. While any element of Array 1 is active, the ports of the elements of Array 2 are sensed during T_s successively by Switch 2 (Sw2). The period separating two consecutive sensing intervals is denoted by T_r . Clearly, $T_r \geq T_s$ and $T_t = M_2 T_r$. A measurement cycle during which all element pairs are switched once lasts $M_1 T_t$ seconds. The separation between the beginnings of two consecutive measurement cycles is called the measurement cycle interval and is denoted by T_{cy} . The cycle repetition rate is the ratio $R \doteq \frac{T_{cy}}{M_1 T_t} \geq 1$. Notice that the switching rate T_r^{-1} is related to the measurement cycle rate T_{cy}^{-1} according to $T_r^{-1} = M_1 M_2 R T_{cy}^{-1}$. The guard interval T_g in Fig. 2 is irrelevant in the subsequent investigations. The motivation for introducing this interval can be found in [7]. One measurement run consists of I cycles.

To characterize the SM of a switched array, we first need to define a (spatial) indexing of the array elements which is then kept fixed. The natural element indexing for a uniform linear array is according to the element spatial ordering, starting at one end. Similarly the natural element indexing of a uniform planar array is determined first by the order of the element row and then by the element order inside its row. The SM of an array during one cycle is entirely defined by a permutation of the element indices. Let $\eta_k(i, \cdot)$ denote (the permutation describing) the SM of Array k during the i th cycle. Referring to Fig. 2, the beginning of the interval when the element pair (m_1, m_2) is switched in the i th cycle is $t_{i,m_1,m_2} \doteq (i - \frac{I+1}{2}) T_{cy} + (\eta_1(i, m_1) - \frac{M_1+1}{2}) T_t + (\eta_2(i, m_2) - \frac{M_2+1}{2}) T_r$. Clearly, $\eta_k(i, m_k)$ is the time index of the interval during which the m_k th element of Array k is switched during the i th cycle ($m_k = 1, \dots, M_k$). Hence, $\eta_k(i, \cdot)$ maps a spatial index onto a time index. The inverse mapping $\eta_k^{-1}(i, \cdot)$ (reported on Fig. 2) determines the temporal order in which the elements of Array k are sequentially

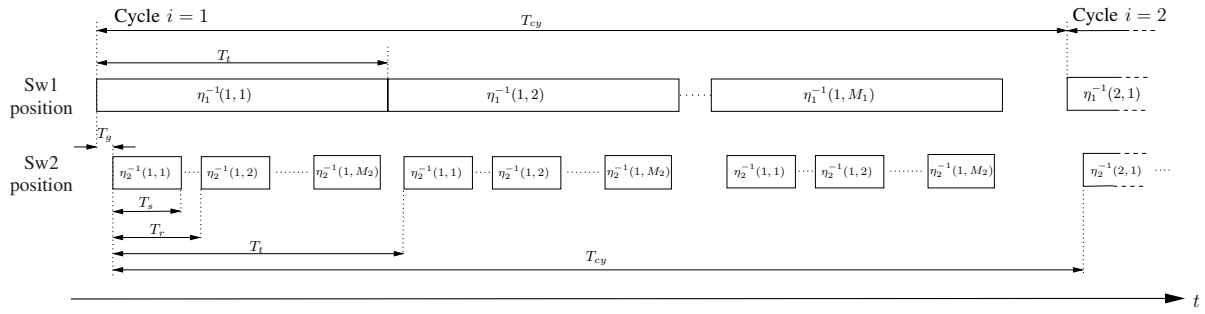


Fig. 2. The considered TDM measurement mode.

switched in the i th cycle. Notice that the SM of Array 2 does not depend on which element of Array 1 is active during each cycle, i.e. $\eta_2(i, \cdot)$ does not depend on m_1 . For notational convenience we identify the permutation $\eta_k(i, \cdot)$ with the vector $\boldsymbol{\eta}_k(i) = [\eta_k(i, m_k), m_k = 1, \dots, M_k]$. If $\boldsymbol{\eta}_k(i) = \boldsymbol{\eta}_k$, $i = 1, \dots, I$, the SM is called cycle-independent. The identity SM $\boldsymbol{\eta}_k = [1, \dots, M_k]$ switches the elements of Array k in their spatial order.

Following the same notation as in [7], the scalar signal at the output of Sw2 reads

$$Y(t) = \sum_{\ell=1}^L s(t; \boldsymbol{\theta}_\ell) + \sqrt{\frac{N_0}{2}} q_2(t) W(t), \quad (3)$$

where $W(t)$ denotes standard complex white Gaussian noise and $q_2(t)$ is an indicator function, i.e. with range $\{0, 1\}$, which takes value one if, and only if, some element of Array 2 is switched by Sw2. Moreover,

$$s(t; \boldsymbol{\theta}_\ell) = \alpha_\ell \exp\{j2\pi\nu_\ell t\} \mathbf{c}_2(\boldsymbol{\Omega}_{2,\ell})^T \mathbf{U}(t; \tau_\ell) \mathbf{c}_1(\boldsymbol{\Omega}_{1,\ell}),$$

where $\mathbf{U}(t; \tau_\ell)$ is the $M_2 \times M_1$ sounding matrix $\mathbf{U}(t; \tau_\ell) \doteq \mathbf{q}_2(t) \mathbf{q}_1(t)^T u(t - \tau_\ell)$, with $u(t)$ denoting the signal at the input of Sw1. The M_2 dimensional vector-valued functions $\mathbf{q}_k(t)$ characterize the timing of Sw k . More specifically, the m_k th entry of $\mathbf{q}_k(t)$ is an indicator function which takes value one, if and only if, Sw k switches the m_k th element of Array k [7].

IV. OBJECTIVE FUNCTION USED IN THE ESTIMATION OF THE DF AND THE DIRECTIONS

A. TDM-MIMO Channel Sounding

According to [7] at each iteration of the ISI-SAGE algorithm, the parameter estimates of the ℓ th path are updated successively in the M-step of the algorithm. This step computes the argument maximizing an objective function $|z(\bar{\boldsymbol{\theta}}_\ell; \hat{x}_\ell)|$, where $\bar{\boldsymbol{\theta}}_\ell \doteq [\boldsymbol{\Omega}_{1,\ell}, \boldsymbol{\Omega}_{2,\ell}, \tau_\ell, \nu_\ell]$ and $|\cdot|$ denotes the norm of the scalar or the vector given as an argument. Notice that the objective function coincides with the maximum-likelihood estimate (MLE) of $\bar{\boldsymbol{\theta}}_\ell$ in a one-path scenario, in which case $\hat{x}_\ell(t) = y(t)$. The function $z(\bar{\boldsymbol{\theta}}_\ell; \hat{x}_\ell)$ is given by

$$z(\bar{\boldsymbol{\theta}}_\ell; \hat{x}_\ell) \doteq \tilde{\mathbf{c}}_2(\boldsymbol{\Omega}_{2,\ell})^H \mathbf{X}_\ell(\tau_\ell, \nu_\ell; \hat{x}_\ell) \tilde{\mathbf{c}}_1(\boldsymbol{\Omega}_{1,\ell})^* \quad (4)$$

with $[\cdot]^H$ denoting the Hermitian operator, $[\cdot]^*$ representing the complex conjugate, and $\tilde{\mathbf{c}}_k(\boldsymbol{\Omega}) \doteq |\mathbf{c}_k(\boldsymbol{\Omega})|^{-1} \mathbf{c}_k(\boldsymbol{\Omega})$ being the normalized response of Array k . The entries of the $M_2 \times M_1$ dimensional matrix $\mathbf{X}(\tau_\ell, \nu_\ell; \hat{x}_\ell)$ read

$$X_{\ell, m_2, m_1}(\tau_\ell, \nu_\ell; \hat{x}_\ell) = \sum_{i=1}^I \left[\exp\{-j2\pi\nu_\ell t_{i, m_1, m_2}\} \right.$$

$$\left. \cdot \int_0^{T_s} u^*(t - \tau_\ell) \exp\{-j2\pi\nu_\ell t\} \hat{x}_\ell(t + t_{i, m_1, m_2}) dt \right], \quad (5)$$

$m_k = 1, \dots, M_k$, $k = 1, 2$. In (5) $\hat{x}_\ell(t) = y(t) - \sum_{\ell'=1, \ell' \neq \ell}^L s(t; \hat{\boldsymbol{\theta}}_{\ell'})$, with $\hat{\boldsymbol{\theta}}_{\ell'}$ denoting the current estimate of $\boldsymbol{\theta}_{\ell'}$, is an estimate of the so-called admissible hidden data $X_\ell(t) = s(t; \boldsymbol{\theta}_\ell) + \sqrt{\frac{N_0}{2}} q_2(t) W(t)$ calculated in the expectation (E-) step of the ISI-SAGE algorithm. The reader is referred to [8] for the properties of the SAGE algorithm and the related terminology.

In the subsequent analysis of the behavior of the objective function versus the DF, the DoD and DoA we make the following four simplifying assumptions: (A) The antenna elements are isotropic; (B) The phase change due to the DF within T_s is neglected, i.e. the term $\exp\{-j2\pi\nu_\ell t\}$ in (5) is set equal to 1. As shown in [1] this effect can be easily included into the model and its impact on the performance of the DF estimate proves to be negligible; (C) We assume that the remaining interference contributed by the waves ℓ' , $\ell' = \{1, \dots, L\} \setminus \{\ell\}$ in the estimate $\hat{x}_\ell(t)$ computed in the E-step of Path ℓ is negligible, i.e. $\hat{x}_\ell(t) = s(t; \boldsymbol{\theta}_\ell) + \sqrt{\frac{N_0}{2}} q_2(t) W(t)$. Under this assumption, the M-step of Path ℓ is derived based on an equivalent signal model where only Path ℓ is present. If we further focus the attention on one particular path, which without loss of generality is selected to be Path 1, then (3) with $L = 1$ is the equivalent signal model for the derivation of the M-step of Path 1. In this case, $\hat{x}_1(t) = y(t)$ and the MLE of $\bar{\boldsymbol{\theta}}_1$ is computed in the M-step. For notational convenience we shall drop the indexing for the parameters of Path 1 in the sequel; (D) As the focus is on the estimation of the DF, DoD, and DoA, we further assume that the ISI-SAGE algorithm has perfectly estimated the delay of Path 1 or has knowledge of it. As a result $z(\bar{\boldsymbol{\theta}}; y)$ reduces to a function of $\boldsymbol{\Omega}_1$, $\boldsymbol{\Omega}_2$, and ν according to

$$z(\nu, \boldsymbol{\Omega}_1, \boldsymbol{\Omega}_2; y) = \sum_{i=1}^I \sum_{m_2=1}^{M_2} \sum_{m_1=1}^{M_1} \tilde{\mathbf{c}}_{1, m_1}(\boldsymbol{\Omega}_1)^* \tilde{\mathbf{c}}_{2, m_2}(\boldsymbol{\Omega}_2)^* \cdot \exp\{-j2\pi\nu t_{i, m_1, m_2}\} \int_0^{T_s} u(t - \tau')^* y(t + t_{i, m_1, m_2}) dt. \quad (6)$$

The notation $(\cdot)'$ designates the true value of the parameter given as an argument.

Under the above assumptions, by dropping a constant term and normalizing by $\frac{1}{I M_1 M_2}$, (6) can be cast as

$$z(\nu, \boldsymbol{\Omega}_1, \boldsymbol{\Omega}_2; y) = \sum_{i=1}^I R_i(\nu) S_i(\tilde{\boldsymbol{\Omega}}_1, \nu) T_i(\tilde{\boldsymbol{\Omega}}_2, \nu) + V(\nu, \boldsymbol{\Omega}_1, \boldsymbol{\Omega}_2) \quad (7)$$

with the notational convention $(\check{\cdot}) \doteq (\cdot)' - (\cdot)$. Moreover,

$$\begin{aligned}
R_i(\tilde{\nu}) &\doteq \frac{1}{T} \exp\{j2\pi\tilde{\nu} (i - \frac{I+1}{2}) T_{cy}\}, \\
S_i(\tilde{\Omega}_1, \tilde{\nu}) &\doteq \frac{1}{M_1} \sum_{m_1=1}^{M_1} \exp\left\{j2\pi \frac{\tilde{\Omega}_1^T \mathbf{r}_{1,m_1}}{\lambda_0} \right. \\
&\quad \left. + j2\pi\tilde{\nu} (\eta_1(i, m_1) - \frac{M_1+1}{2}) T_t\right\}, \\
T_i(\tilde{\Omega}_2, \tilde{\nu}) &\doteq \frac{1}{M_2} \sum_{m_2=1}^{M_2} \exp\left\{j2\pi \frac{\tilde{\Omega}_2^T \mathbf{r}_{2,m_2}}{\lambda_0} \right. \\
&\quad \left. + j2\pi\tilde{\nu} (\eta_2(i, m_2) - \frac{M_2+1}{2}) T_r\right\}. \quad (8)
\end{aligned}$$

The noise term $V(\nu, \Omega_1, \Omega_2)$ can be derived analogously to $V(\nu)$ in [1]. Notice that the expressions in the arguments of the exponential terms in the summands of $S_i(\tilde{\Omega}_1, \tilde{\nu})$ and $T_i(\tilde{\Omega}_2, \tilde{\nu})$ reveal respectively a coupling depending on $\eta_1(i, \cdot)$ in the estimation of the DoD and the DF and a coupling depending on $\eta_2(i, \cdot)$ in the estimation of the DoA and the DF.

B. Case Study: TDM-SIMO Channel Sounding with Uniform Linear Array

In this subsection we investigate in detail the above mentioned coupling and in particular how the SM affects the objective function of the DF and direction MLEs. To keep the discussion simple we restrict the attention to a special case where Array 1 consists of one element ($M_1 = 1$) and Array 2 is uniform and linear. In this case, the DoD cannot be estimated and (7) reduces to

$$z(\nu, \Omega_2; y) = \sum_{i=1}^I R_i(\tilde{\nu}) T_i(\tilde{\Omega}_2, \tilde{\nu}) + V(\nu, \Omega_2). \quad (9)$$

We investigate the behavior of the absolute value of (9) in the noiseless case ($V(\nu, \Omega_2) = 0$). Array 2 consists of M_2 equidistant isotropic elements with locations $\mathbf{r}_{2,m_2} = [\frac{m_2\lambda_0}{2}, 0, 0]^T$, $m_2 = 1, \dots, M_2$. The inner products arising in the response of this array are calculated as $\tilde{\Omega}_2^T \mathbf{r}_{2,m_2} = \omega \frac{m_2\lambda_0}{2}$, $m_2 = 1, \dots, M_2$, where $\omega \doteq \cos(\phi_2) \sin(\theta_2)$. The parameter ω can be interpreted as a spatial frequency. It can be also written as $\omega = \cos(\psi)$ where ψ is the angle between the impinging direction and the array axis. This angle is the only characteristic of the incident direction that can be uniquely determined with a linear array.

The absolute value of (9) reads in this case

$$|z(\nu, \Omega_2; y)| = |z(\tilde{\nu}, \tilde{\omega}; y)|. \quad (10)$$

If the SM is cycle-independent, the right-hand expression in (10) factorizes according to

$$|z(\tilde{\nu}, \tilde{\omega}; y)| = |G(\tilde{\nu})| \cdot |T(\tilde{\omega}, \tilde{\nu})|, \quad (11)$$

where

$$\begin{aligned}
G(\tilde{\nu}) &\doteq \frac{\sin(\pi\tilde{\nu}IT_{cy})}{I \sin(\pi\tilde{\nu}T_{cy})}, \\
T(\tilde{\omega}, \tilde{\nu}) &\doteq \frac{1}{M_2} \sum_{m_2=1}^{M_2} \exp\{jm_2\pi\tilde{\omega} + j2\pi\tilde{\nu}[\eta_2(m_2) - \frac{M_2+1}{2}]T_r\}.
\end{aligned}$$

We investigate the impact of different SMs on (11) for the setting of the TDM-SIMO system and the one-wave scenario specified in Table I. The wave is incident perpendicular to the array axis and its DF is 0 Hz. Notice that from (10) the behaviour of the objective function only depends on the DF deviation from the true DF so that the choice of the latter within the range $(-\frac{1}{2T_r}, \frac{1}{2T_r}]$ is irrelevant. Fig. 3(a), 3(b), and 3(c) depict the graphs of respectively $|G(\tilde{\nu})|$, $|T(\tilde{\omega}, \tilde{\nu})|$, and $|z(\tilde{\nu}, \tilde{\omega}; y)|$ in (11), when the conventionally used identity

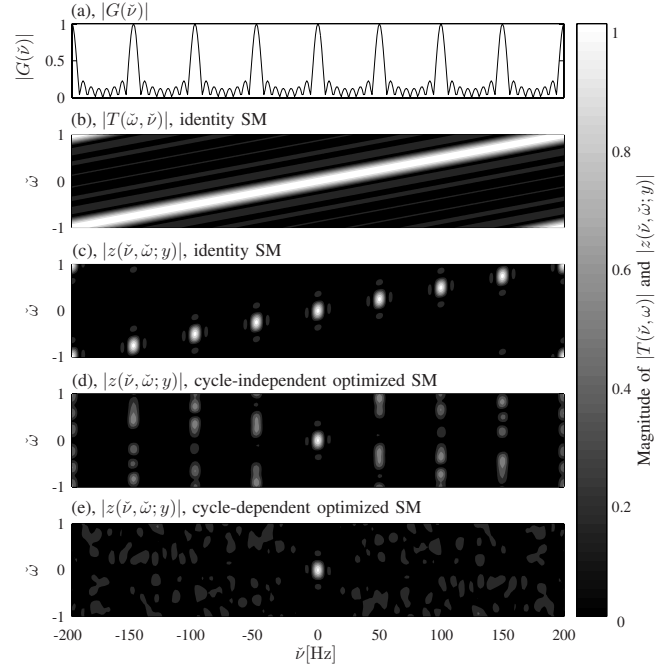


Fig. 3. Objective functions for the joint DF and DoA MLEs in the case study (TDM-SIMO with uniform linear array) where the following SMs are selected: $\eta_2 = [1, 2, \dots, 8]$ (c), $\eta_2(i) = [4, 2, 1, 8, 5, 7, 3, 6]$ (d), and a randomly selected cycle-dependent SM (e). Fig. 3 (a) and (b) depict the factors of the objective function (see (11)) for the identity SM.

SM, is applied. Notice that the range of $\tilde{\nu}$ is $(-\frac{1}{2T_r}, \frac{1}{2T_r}] = (-200, 200]$ Hz.

Clearly, the period of $|G(\tilde{\nu})|$ is $\frac{1}{T_{cy}} = 50$ Hz. The loci of the pairs $(\tilde{\nu}, \tilde{\omega})$ where $|T(\tilde{\omega}, \tilde{\nu})|$ equals its maximum value ($= 1$) is the line $\tilde{\omega} = \tilde{\nu}T_r$. As can be observed in Fig. 3 (c) the product of these two functions, i.e. $|z(\tilde{\nu}, \tilde{\omega}; y)|$, exhibits multiple maxima along the above line separated by $\frac{1}{T_{cy}}$ in $\tilde{\nu}$. These multiple maxima cause an ambiguity in the joint ML estimation of the DF and DoA when the DFER is selected equal to $(-\frac{1}{2T_r}, \frac{1}{2T_r}]$. Notice that $|z(\tilde{\nu}, \tilde{\omega}; y)|$ exhibits one unique maximum if $\tilde{\nu} \in (-\frac{1}{2T_{cy}}, \frac{1}{2T_{cy}}]$. Thus, if this SM is used, the DFER has to be restricted to the above interval in order to avoid the ambiguity problem.

Fig. 3(d) and Fig. 3(e) report respectively the graphs of $|z(\tilde{\nu}, \tilde{\omega}; y)|$ for the cycle-independent SM $\eta_2 = [4, 2, 1, 8, 5, 7, 3, 6]$ and a cycle-dependent randomly selected SM. With this selection of the SMs, $|z(\tilde{\nu}, \tilde{\omega}; y)|$ exhibits a unique maximum and therefore the ambiguity problem does not occur. One can still see clearly the impact of the periodic behavior of $|G(\tilde{\nu})|$ on the objective function depicted in Fig. 3(d) as side-lobe stripes at the loci of the maxima of $|G(\tilde{\nu})|$ when the SM is cycle-independent. As exemplified by Fig. 3(e) this pattern vanishes completely when using a cycle-dependent SM. Furthermore, the side-lobes of the third depicted objective function have much lower magnitude than those of the second objective function.

This study shows that in the worst case (using the identity SM), the operational DFER is $(-\frac{1}{2T_{cy}}, \frac{1}{2T_{cy}}]$. By appropriately selecting the SM the DFER can be extended to $(-\frac{1}{2T_r}, \frac{1}{2T_r}]$, i.e., by a factor $M_2 = 8$ in this case study or in general by $M_1 M_2 R$. Furthermore, Fig. 3(c)–(e) make it evident that the SMs significantly affect the magnitudes of the side-lobes of the

TABLE I
CASE STUDY: SETTING OF THE TDM-SIMO SYSTEM
AND PARAMETERS OF THE INCIDENT WAVE

I	M ₁	M ₂	R	T _{cy} [s]	ν' [Hz]	ω'
8	1	8	1	0.02	0	0

objective function. This impact is investigated in more detail in Section V.

C. Analysis of the Ambiguity Effect for the Case Study

In this subsection we derive a necessary and sufficient condition for a cycle-independent SM to lead to an objective function exhibiting multiple maxima. We also show that modulo-type SMs (and among them the identity SM) cause the ambiguity problem when the cycle repetition rate R is integer.

The function $z(\tilde{\nu}, \tilde{\omega}; y)$ in (10) is of the form $z(\tilde{\nu}, \tilde{\omega}; y) = \frac{1}{IM_2} \sum_{i=1}^I \sum_{m_2=1}^{M_2} \exp\{j\Phi_{i,m_2}\}$, where $\Phi_{i,m_2} \doteq 2\pi\tilde{\nu}(i - \frac{I+1}{2})T_{cy} + 2\pi\tilde{\omega}(\eta_2(i, m_2) - \frac{M_2+1}{2})T_r + \pi\tilde{\omega}m_2$. When $\tilde{\omega} = 0$ and $\tilde{\nu} = 0$, $|z(\tilde{\nu}, \tilde{\omega}; y)|$ equals its maximum value 1. However, a necessary and sufficient condition for $|z(\tilde{\nu}, \tilde{\omega}; y)| = 1$ to hold is that all the phases in the double sum are congruent modulo 2π . This will be the case if, and only if,

$$\begin{aligned} \Phi_{i,m_2} - \Phi_{i+1,m_2} &\equiv 0 \pmod{2\pi} \\ m_2 &= 1, \dots, M_2, \quad i = 1, \dots, I-1 \end{aligned} \quad (12)$$

and

$$\begin{aligned} \Phi_{i,m_2} - \Phi_{i,m_2+1} &\equiv 0 \pmod{2\pi} \\ m_2 &= 1, \dots, M_2-1, \quad i = 1, \dots, I. \end{aligned} \quad (13)$$

Hence $|z(\tilde{\nu}, \tilde{\omega}; y)|$ exhibits multiple maxima if, and only if, the system of equations defined by (12) and (13) has one or more non-trivial solutions $(\tilde{\nu}, \tilde{\omega}) \in (-\frac{1}{2T_r}, \frac{1}{2T_r}] \times [\omega' - 1, \omega' + 1]$. The trivial solution is $(\tilde{\nu}, \tilde{\omega}) = (0, 0)$.

In the sequel, we focus on cycle-independent SMs. In this case $\eta_2(i, m_2) - \eta_2(i+1, m_2) = 0$ and (12) reduces to $\tilde{\nu}T_{cy} = K$ for $K \in \mathbb{Z} \cap (-\frac{RM_2}{2}, \frac{RM_2}{2}]$, where \mathbb{Z} is the set of integers. Inserting this identity in (13) yields

$$K \cdot \frac{\dot{\eta}_2(m_2)}{RM_2} \equiv \frac{\tilde{\omega}}{2} \pmod{1}, \quad m_2 = 1, \dots, M_2-1, \quad (14)$$

where $\dot{\eta}_2(m_2) \doteq \eta_2(m_2) - \eta_2(m_2+1)$. Hence, provided the SM is cycle-independent, a necessary and sufficient condition for the ambiguity problem to occur is that the equation system (14) has at least one non-trivial solution $(K, \tilde{\omega}) \in (\mathbb{Z} \cap (-\frac{RM_2}{2}, \frac{RM_2}{2}]) \times [\omega' - 1, \omega' + 1]$.

A modulo-type SM fulfills the congruence $(\eta_2(m_2) - 1) \equiv Jm_2 + K \pmod{M_2}$ for some $J, K \in \mathbb{Z}$ with J and M_2 being relatively prime. As an example, the commonly used identity SM $\eta_2 = [1, 2, \dots, M_2]$ is a modulo-type SM with $J = 1$ and $K = 0$. For any modulo-type SM, $\{\dot{\eta}_2(m_2); m_2 = 1, \dots, M_2-1\} = \{J, J - M_2\}$. Hence (14) consists of two different congruences. Elimination of $\tilde{\omega}$ yields $K = RK'$, with K' taking any value in $\mathbb{Z} \cap (-\frac{M_2}{2}, \frac{M_2}{2}]$. When $R \in \mathbb{Z}$, the non-trivial solutions for K are the $RM_2 - 1$ values in $\mathbb{Z} \cap (-\frac{RM_2}{2}, \frac{RM_2}{2}) \setminus \{0\}$. Notice that this result is in accordance with the 8 maxima (corresponding to the 7 non-trivial solutions plus the trivial solution) that can be observed in Fig. 3(c).

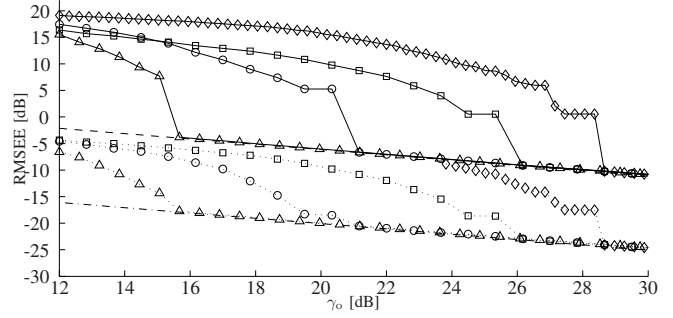


Fig. 4. RMSEs of $\hat{\nu}$ (solid curves) and $\hat{\psi}$ (dotted curves) versus γ_0 computed using the setting given in Table I for different SMs. The dashed and the dash-dotted lines represent the CRLBs of $\hat{\nu}$ and $\hat{\psi}$ respectively. The curves with symbols \diamond , \square , \circ , \triangle have been obtained using 3 cycle-independent SMs and 1 cycle-dependent SM leading to NSL = 0.85, 0.80, 0.58, and 0.28 respectively.

V. PERFORMANCE SIMULATIONS

The theoretical investigations of the study case reported in the previous subsection show that the SM strongly affects the side-lobes of the objective function of the DF and DoA MLEs. As a consequence the SM will also affect the robustness of the estimators toward noise since this robustness directly depends on the magnitudes of the side-lobes.

We define the normalized side-lobe level (NSL) associated with a SM to be the magnitude of the highest side-lobe of the corresponding objective function. It is obvious that objective functions with NSL equal to one have multiple maxima and therefore lead to an ambiguity in the estimation of DF and DoA, whereas objective functions with NSL less than 1 have a unique maximum.

We show by means of Monte-Carlo simulations that the NSL associated with a SM can be used as a figure of merit of this SM for the optimisation of the performance of the DF and DoA MLEs. The parameter setting of the considered scenario is the same as that used in the case study (see Table I). Fig. 4 depicts the RMSEs of the MLEs $\hat{\nu}$ and $\hat{\psi}$ versus the output signal-to-noise ratio $\gamma_0 \doteq IM_2P|\alpha|^2|c_1(\Omega_1)|^2|c_2(\Omega_2)|^2/(\frac{N_0}{T_s})$ [1] for four SMs leading to NSLs equal to 0.28, 0.58, 0.80, and 0.85 respectively. The symbol P in the above expression denotes the transmitted signal power. The RMSEs are compared to the corresponding individual Cramér-Rao lower bounds (CRLBs) calculated in [8] assuming parallel SIMO channel sounding.

As shown in Fig. 4 all curves exhibit the same behavior, i.e. when γ_0 is larger than a certain threshold, γ_0^{th} , the RMSEs of $\hat{\nu}$ and $\hat{\psi}$ are close to the corresponding CRLBs. When $\gamma_0 < \gamma_0^{\text{th}}$, the RMSEs increase dramatically as already shown in [1]. Further simulations show that γ_0^{th} increases along with the NSL. This behavior can be explained as follows: The probability of the event that the maximum of any side-lobe of the objective function is higher than the maximum of its main-lobe is larger when these side-lobes have high magnitudes. Notice that the threshold effect is well-known in non-linear estimation such as frequency estimation [9].

We can use the RMSEE curve of the DF MLE under the hypothesis that all other parameters but the complex gain of the path are known as a benchmark for the DF MLE performance when all path parameters are unknown. This curve is indeed a lower bound for the RMSEE curve of the latter DF estimates. Monte Carlo simulations not reported here show that this benchmark curve exhibits a threshold $\gamma_0^{\text{th}} = 15$ dB and is

TABLE II
SETTINGS OF THE CHANNEL SOUNDER FOR
MEASUREMENT SCENARIOS I AND II

Parameters	Scenario I	Scenario II
SM at Array 2	Patch-wise identity SM	Patch-wise optimized SM
T_r [μ s]	3.05	5.10
T_{cy} [ms]	6.2	47.2
Selected DFER [Hz]	$(-\frac{1}{2T_{cy}}, \frac{1}{2T_{cy}}] = (-81.3, 81.3]$	$(-\frac{1}{2T_r}, \frac{1}{2T_r}] = (-98\ 039, 98\ 039]$

close to the CRLB of $\hat{\nu}$ for $\gamma_o > \gamma_o^{\text{th}}$. From Fig. 4 we observe that the threshold γ_o^{th} of the RMSEE curve of $\hat{\nu}$ obtained for the SM leading to NSL=0.28 is 0.5 dB apart from that of the benchmark curve. Hence, the former threshold is close to the minimum achievable threshold. This observation confirms that the NSL is a suitable figure of merit for the selection of “good” SMs, i.e. leading to MLEs operating close to optimum.

VI. EXPERIMENTAL INVESTIGATIONS

In this section, we present experimental investigations that illustrate the impact of the SM on the objective function used in the ISI-SAGE algorithm to estimate the DF and DoA of propagation paths based on measurement data. The measurements were performed with the TDM-MIMO channel sounder PROPSound [10]. The Tx array consisted of 3 conformal sub-arrays of 8 dual-polarized patches uniformly spaced on a cylinder together with a uniform rectangular 2×2 sub-array of 4 dual-polarized patches placed on top of the cylinder ($M_1=54$). At the Rx a 4×4 planar array with 16 dual-polarized patches was used ($M_2=32$). The spacing between the Rx array elements and the elements of the four Tx sub-arrays is half a wavelength. The selected carrier frequency was 2.45 GHz. The sounding signal was a pseudo-noise (PN) sequence of length $K=255$ chips with chip duration $T_c=10$ ns. The sensing interval coincided with one period of the PN-sequence, i.e. $T_s=KT_c=2.55$ μ s. The transmitted power was 100 mW.

The Rx array was mounted outside a window on the 3rd floor of the Elektrobit AG building in Bubikon, Switzerland. The Tx array was mounted on the roof of a van moving with approximately 8 m/s away from the building. The measurements were performed twice along the same route with different settings of the sounding equipment (see Table II). The van was driving at approximately the same velocity during both measurement recordings to ensure propagation scenarios with almost identical DFs. The azimuth of arrival (AoA), the elevation of arrival (EoA) and the DF of the LOS path can be calculated from the location of the Rx as well as the position and the velocity of the van to be approximately 5° , 20° and -59 Hz respectively. The two settings of the sounding equipment were selected in such a way that the maximum DF is in $(-\frac{1}{2T_{cy}}, \frac{1}{2T_{cy}}]$ in Scenario I and outside this range but in $(-\frac{1}{2T_r}, \frac{1}{2T_r}]$ in Scenario II. These intervals were then selected as the corresponding DFERs for the two scenarios. As explained later, the SM at the Tx is irrelevant in the investigated situation. At the Rx, we apply a patch-wise identity SM in Scenario I and a patch-wise optimized SM in Scenario II. The term “patch-wise” indicates that the two elements of each patch are always switched consecutively. This is done to mitigate phase noise effect for accurate polarization estimation.

The ISI-SAGE algorithm is applied to the measurement data to estimate the individual parameter vectors of $L=4$ propagation paths using $I=4$ measurement cycles. The parameter estimates of the four paths are initialized successively with a Non-Coherent Maximum Likelihood (NC-ML) technique described in [3]. Once the initialization is completed, the E- and M-steps of the ISI-SAGE are performed as described in [7]. It can be shown that the objective function used for the joint initialization of $\hat{\nu}_\ell$ and $\hat{\Omega}_{2,\ell}$ after the initial delay estimate $\hat{\tau}_\ell(0)$ has been computed is similar to the absolute value of (9) with $\tau_\ell = \hat{\tau}_\ell(0)$ and $\hat{x}_\ell(t) = y(t) - \sum_{\ell'=1}^{\ell-1} s(t; \hat{\theta}_{\ell'}(0))$. Since at that stage, the DoD of the ℓ th path has not been estimated yet, the NC-ML technique is used to initialize $\hat{\nu}_\ell$ and $\hat{\Omega}_{2,\ell}$ jointly. The SM at the Tx is irrelevant when this method is applied. Hence, we can use the initialization procedure of the ISI-SAGE algorithm to experimentally investigate scenarios similar to the case study described in Subsection IV-B. The differences between the experimental scenarios and the case study are as follows: (1) the SIMO antenna system considered in the case study is replaced by a MIMO system in the experimental scenario; (2) a uniform planar array with dual-polarized elements is used instead of a uniform linear array; (3) the array elements are not isotropic; (4) in the calculation of $\hat{x}_\ell(t)$ the contribution of the waves but the ℓ th one were either not or only partially cancelled.

In the sequel we restrict the attention to the LOS path indexed $\ell=1$. To visualize the behavior of the objective function versus ν_1 , we compute $F(\nu_1) \doteq \max_{\tilde{\Omega}_{2,1}} |z(\nu_1, \tilde{\Omega}_{2,1}; \hat{x}_1 = y)|^2$ with $z(\nu_1, \tilde{\Omega}_{2,1}; y)$ given in (9). Notice that $T_i(\tilde{\Omega}_{2,1}, \tilde{\nu}_1)$ (see (8)) depends on the real response of the Rx array, i.e. includes the radiation patterns of the elements in the array. Inserting (9) with the noise term omitted in the definition of $F(\nu_1)$ we obtain

$$\begin{aligned} F(\nu_1) &= \max_{\tilde{\Omega}_{2,1}} \left| \sum_{i=1}^I R_i(\tilde{\nu}_1) T_i(\tilde{\Omega}_{2,1}, \tilde{\nu}_1) \right|^2 \\ &= \max_{\tilde{\Omega}_{2,1}} |G(\tilde{\nu}_1) T(\tilde{\Omega}_{2,1}, \tilde{\nu}_1)|^2 \\ &= |T'(\tilde{\nu}_1)|^2 \cdot |G(\tilde{\nu}_1)|^2 \end{aligned} \quad (15)$$

with $T'(\tilde{\nu}_1) \doteq \max_{\tilde{\Omega}_{2,1}} T(\tilde{\Omega}_{2,1}, \tilde{\nu}_1)$. The second line follows similarly to (11) since the SM is cycle-independent. Hence, the SM only affects $F(\nu_1)$ via $|T'(\tilde{\nu}_1)|^2$.

The right hand expression in (15) will be useful for understanding the behavior of $F(\nu_1)$ computed from the measurement data. This function is plotted versus ν_1 ranging in $(-81.3 \text{ Hz}, 81.3 \text{ Hz}]$ in Fig. 5 (top) for both scenarios. The pulse-train-like behavior of the curves is due to the factor $|G(\tilde{\nu}_1)|^2$ in (15), which is periodic with period $1/T_{cy}$. The maximum of $F(\nu_1)$ in Scenario I (with DFER $(-\frac{1}{2T_{cy}}, \frac{1}{2T_{cy}}]$), is located at -52 Hz. In Scenario II (with DFER $(-\frac{1}{2T_r}, \frac{1}{2T_r}]$) the maximum of $F(\nu_1)$ is located at -81 Hz. Notice that these values are the initial DF estimates of the LOS path returned by the ISI-SAGE algorithm. After four iterations of the algorithm the DF estimates of the LOS path have converged to -52.5 Hz, and the AoA and EoA estimates equal 4.6° and 27° respectively in Scenario I. In Scenario II the DF estimate converges to -60 Hz, and the AoA and EoA estimates equal 5.3° and 18.7° respectively. All these values are in accordance with the theoretically calculated values. The deviation between

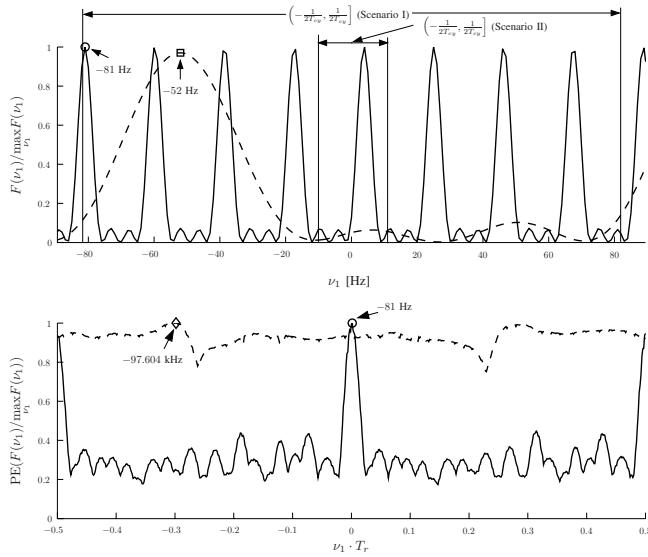


Fig. 5. Normalized $F(\nu_1)$ (top) and pseudo-envelope $PE(F(\nu_1))$ (bottom) computed from the measurement data obtained in Scenario I (dashed lines) and Scenario II (solid lines). The marks \square and \diamond denote the maxima of $F(\nu_1)$ in Scenario I when the DFER is respectively $(-\frac{1}{2T_r}, \frac{1}{2T_r})$ and extended to $(-\frac{1}{2T_r}, \frac{1}{2T_r})$. The mark \circ denotes the maximum of $F(\nu_1)$ in Scenario II (DFER = $(-\frac{1}{2T_r}, \frac{1}{2T_r})$).

the two sets of the estimates is due to the difference in the velocities and the positions of the van during the measurement recordings.

The pulse-train-behavior of $F(\nu_1)$ due to $|G(\nu_1)|^2$ makes it difficult to visualize the effect of the SM (embodied in $|T'(\tilde{\nu}_1)|^2$) on the former function when $\tilde{\nu}$ ranges in $(-\frac{1}{2T_r}, \frac{1}{2T_r})$. To circumvent this problem we compute an approximation of $|T'(\tilde{\nu}_1)|$ from $F(\nu_1)$ as follows: $PE(F(\nu_1))$ is a pseudo-envelope (PE) obtained by dividing the range of ν_1 into multiple bins with equal width of $\frac{1}{T_{cy}}$ and connecting the maxima of $F(\nu_1)$ within each bin using linear interpolation. Fig. 5 (bottom) reports the computed PE curves for both scenarios. For Scenario I, $PE(F(\nu_1))$ remains close to one over the entire range $(-\frac{1}{2T_r}, \frac{1}{2T_r})$. This behavior is due to the identity SM used for the 4×4 planar array. In Scenario II, $PE(F(\nu_1))$ exhibits a dominant lobe and multiple side-lobes with significant lower amplitude. The width of the main lobe is in accordance with the analytically derived value of $\frac{2}{M_2} \frac{1}{T_r}$ for the separation between the zero points of the main lobe.

In case the DFER is extended to $(-\frac{1}{2T_r}, \frac{1}{2T_r})$ in Scenario I, the maximum of $F(\nu_1)$ is located at -97.604 kHz in the initialization step (as shown in Fig. 5 (bottom)), and stays at this value after 4 iterations. The AoA and EoA estimates are respectively 70° and 2° . These estimates are obviously artifacts that result due to the identity SM used at the Rx array.

Notice that the high side-lobes at the boundary of the DF estimation range are due to the patch-wise switching of the arrays. When the DF is very low compared to the switching rate as it is the case here, the resulting phase-shift due to the DF between consecutive sensing intervals of the elements of a patch is close to zero, which leads to an effective doubling of T_r . As a result, the graph of $PE(F(\nu_1))$ exhibits two segments of similar shape as shown in Fig. 5 (bottom).

The above investigations show experimentally the ambiguity effect that occurs when the DFER is extended to $(-\frac{1}{2T_r}, \frac{1}{2T_r})$

and the identity SM combined with a planar array is used. It also demonstrates that this problem is avoided by appropriately selecting the SM.

VII. CONCLUSION

In this contribution we investigate the behavior of the Doppler frequency (DF) and direction estimates obtained with the ISI-SAGE algorithm [2] and [3] when the scheme is used in combination with TDM-MIMO channel sounding.

Theoretical analysis combined with simulations show that when the DF estimation range (DFER) is selected to be from minus to plus half the switching rate as proposed in [1] the switching modes (SMs) of the arrays have to be selected suitably. It is shown that traditionally used SMs of uniform linear and planar arrays where the elements are switched according to their natural spatial ordering are inappropriate as they lead to an ambiguity in the joint estimation of DF and directions. The investigations also reveal that the objective function of the DF and direction estimates and in particular the levels of its side-lobes are strongly affected by the choice of the SM.

We propose to associate to any SM the so-called normalized side-lobe level (NSL) of the objective function resulting from selecting this SM. Monte Carlo simulations show that the NSL is a sensible figure of merit for the identification of SMs leading to DF and direction estimates performing close to optimum in terms of root mean square estimation error.

The above theoretical studies are confirmed by experimental investigations using the ISI-SAGE algorithm. These investigations show that consecutive switching of the two elements of dual polarized patches in an array reduce the DFER by a factor two. However this reduction is in practice irrelevant as the switching rate implemented in measurement equipments is usually several orders of magnitude larger than the maximum Doppler frequency observable in radio propagation environments.

REFERENCES

- [1] X. Yin, B. H. Fleury, P. Jourdan, and A. Stucki, "Doppler frequency estimation for channel sounding using switched multiple transmit and receive antennae," *Proc. IEEE Global Communications Conference, Globecom2003*, vol. 4, pp. 2177–2181, 2003.
- [2] B. H. Fleury, X. Yin, P. Jourdan, and A. Stucki, "High-resolution channel parameter estimation for communication systems equipped with antenna arrays," *Proc. 13th IFAC Symposium on System Identification (SYSID 2003)*, Rotterdam, The Netherlands, no. ISC-379, 2003.
- [3] X. Yin, B. H. Fleury, P. Jourdan, and A. Stucki, "Polarization estimation of individual propagation paths using the SAGE algorithm," *The 14th IEEE International Symposium on Personal, Indoor and Mobile Radio Communications, PIMRC2003*, vol. 2, pp. 1795–1799, 2003.
- [4] I. E. Telatar, "Capacity of multi-antenna Gaussian channels," *European Transactions on Telecommunication*, vol. 10, pp. 585–595, 1999.
- [5] G. J. Foschini and M. J. Gans, "On limits of wireless communications in a fading environment when using multiple antennas," *Wireless Personal Communications*, vol. 6, pp. 311–335, 1998.
- [6] D. Chizhik, G. J. Foschini, and R. A. Valenzuela, "Capacities of multi-element transmit and receive antennas: Correlations and keyholes," *IEEE Electronics Letters*, vol. 36, no. 13, pp. 1099–1100, June 2000.
- [7] B. H. Fleury, P. Jourdan, and A. Stucki, "High-resolution channel parameter estimation for MIMO applications using the SAGE algorithm," *Proceedings of Int. Zurich Seminar on Broadband Communications 2002*, vol. 30, pp. 1–9, 2002.
- [8] B. H. Fleury, M. Tschudin, R. Heddergott, D. Dahlhaus, and K. L. Pedersen, "Channel parameter estimation in mobile radio environments using the SAGE algorithm," *IEEE Journal on Selected Areas in Communications*, vol. 17, no. 3, pp. 434–450, Mar. 1999.
- [9] D. C. Rife and R. R. Boorstyn, "Single tone parameter estimation from discrete-time observations," *IEEE Trans. Information Theory*, 1974.
- [10] A. Stucki et al., "PROPSound System Specifications Document: Concept and Specifications," Elektrobit AG, Switzerland, Internal Report, 2001.